Roman Kostecki, Heike Ebendorff-Heidepriem, Shahraam Afshar V., Grant McAdam, Claire Davis, and Tanya M. Monro

Novel polymer functionalization method for exposed-core optical fiber

Optical Materials Express, 2014; 4(8):1515-1525

A Novel Polymer Functionalization Method for Exposed-Core Optical Fiber

Roman Kostecki,[1]* Heike Ebendorff-Heidepriem,[1] Shahraam Afshar V.,[1] Grant McAdam,[2] Claire Davis,[2] and Tanya M. Monro[1]

[1]*ARC Centre of Excellence for Nanoscale BioPhotonics, and Institute for Photonics and Advanced Sensing, and the School of Chemistry and Physics, The University of Adelaide, Adelaide, South Australia, 5005, Australia*
[2]*Defence Science and Technology Organisation, Fishermans Bend, Victoria, Australia*
*roman.kostecki@adelaide.edu.au

Abstract: We report on a one step functionalization process for optical fiber sensing applications in which a thin film (∼50 nm) polymer doped with sensor molecules is applied to a silica exposed-core fiber. The method removes the need for surface attachment of functional groups, while integrating the polymer, silica and sensor molecule elements to create a distributed sensor capable of detecting an analyte of interest anywhere along the fiber's length. We also show that the thin film coating serves a protective function, reducing deterioration in the transmission properties of the silica exposed-core fiber, but increasing loss.

OCIS codes: (060.2270) Fiber characterization; (060.2280) Fiber design and fabrication; (060.2370) Fiber optics sensors; (060.4005) Microstructured fibers; (160.2540) Fluorescent and luminescent materials; (220.4241) Nanostructure fabrication; (280.1545) Chemical analysis; (280.4788) Optical sensing and sensors; (290.5880) Scattering, rough surfaces; (300.2530) Fluorescence, laser-induced; (310.1860) Deposition and fabrication; (310.2785) Guided wave applications; (310.6628) Subwavelength structures, nanostructures; (310.6845) Thin film devices and applications.

References and links

1. R. Kostecki, H. Ebendorff-Heidepriem, C. Davis, G. McAdam, S. C. Warren-Smith, and T. M. Monro, "Silica exposed-core microstructured optical fibers," Opt. Mater. Express **2**, 1538 – 1547 (2012).
2. T. M. Monro, D. J. Richardson, and P. J. Bennett, "Developing holey fibres for evanescent field devices," Electron. Lett. **35**, 1188 – 1189 (1999).
3. S. Afshar V., S. C. Warren-Smith, and T. M. Monro, "Enhancement of fluorescence-based sensing using microstructured optical fibres," Opt. Express **15**, 17891 – 17901 (2007).
4. O. S. Wolfbeis, "Fiber-optic chemical sensors and biosensors," Anal. Chem. **80**, 4269 – 4283 (2008).
5. T. M. Monro, S. Warren-Smith, E. P. Schartner, A. François, S. Heng, H. Ebendorff-Heidepriem, and S. Afshar V., "Sensing with suspended-core optical fibers," Opt. Fiber Technol. **16**, 343 – 356 (2010).
6. C. Lodeiro, J. L. Capelo, J. C. Mejuto, E. Oliveira, H. M. Santos, B. Pedras, and C. Nunez, "Light and colour as analytical detection tools: A journey into the periodic table using polyamines to bio-inspired systems as chemosensors," Chem. Soc. Rev. **39**, 2948 – 2976 (2010).
7. S. Heng, M.-C. Nguyen, R. Kostecki, T. M. Monro, and A. D. Abell, "Nanoliter-scale, regenerable ion sensor: sensing with a surface functionalized microstructured optical fibre," RSC Adv. **3**, 8308 – 8317 (2013).
8. H. T. C. Foo, H. Ebendorff-Heidepriem, C. J. Sumby, and T. M. Monro, "Towards microstructured optical fibre sensors: surface analysis of silanised lead silicate glass," J. Mater. Chem. C **1**, 6782 – 6789 (2013).
9. B. Sciacca, A. François, M. Klingler-Hoffmann, J. Brazzatti, M. Penno, P. Hoffmann, and T. M. Monro, "Radiative-surface plasmon resonance for the detection of apolipoprotein E in medical diagnostics applications," Nanomed. - NBM **9**, 550 – 557 (2013).
10. A. François, H. Ebendorff-Heidepriem, C. J. Sumby, and T. M. Monro, "Comparison of surface functionalization processes for optical fibre biosensing applications," in "20th International Conference on Optical Fibre Sensors," vol. 7503 of *Proc. SPIE* (2009).

11. S. C. Warren-Smith, S. Heng, H. Ebendorff-Heidepriem, A. D. Abell, and T. M. Monro, "Fluorescence-based aluminum ion sensing using a surface-functionalized microstructured optical fiber," Langmuir **27**, 5680 – 5685 (2011).
12. M. Zhu, M. Z. Lerum, and W. Chen, "How to prepare reproducible, homogeneous, and hydrolytically stable aminosilane-derived layers on silica," Langmuir **28**, 416 – 423 (2012).
13. K. Richardson, D. Krol, and K. Hirao, "Glasses for photonic applications," Int. J. Appl. Glass Sci. **1**, 74 – 86 (2010).
14. K. Peters, "Polymer optical fiber sensors - a review," Smart Mater. Struct. **20**, 013002 (2011).
15. S. H. Law, M. A. van Eijkelenborg, G. W. Barton, C. Yan, R. Lwin, and J. Gan, "Cleaved end-face quality of microstructured polymer optical fibres," Opt. Commun. **265**, 513 – 520 (2006).
16. S. Atakaramians, K. Cook, H. Ebendorff-Heidepriem, S. Afshar V., J. Canning, D. Abbott, and T. M. Monro, "Cleaving of extremely porous polymer fibers," IEEE Photon. J. **1**, 286 – 292 (2009).
17. A. Stefani, K. Nielsen, H. K. Rasmussen, and O. Bang, "Cleaving of TOPAS and PMMA microstructured polymer optical fibers: Core-shift and statistical quality optimization," Opt. Commun. **285**, 1825 – 1833 (2012).
18. M. Li and D. A. Nolan, "Optical transmission fiber design evolution," J. Lightwave Technol. **26**, 1079 – 1092 (2008).
19. E. P. Schartner, H. Ebendorff-Heidepriem, S. C. Warren-Smith, R. T. White, and T. M. Monro, "Driving down the detection limit in microstructured fiber-based chemical dip sensors," Sensors **11**, 2961 – 2971 (2011).
20. S. C. Warren-Smith and T. M. Monro, "Exposed core microstructured optical fiber bragg gratings: refractive index sensing," Opt. Express **22**, 1480 – 1489 (2014).
21. K. J. Rowland, A. François, P. Hoffmann, and T. M. Monro, "Fluorescent polymer coated capillaries as optofluidic refractometric sensors," Opt. Express **21**, 11492 – 11505 (2013).
22. V. V. N. R. Kishore, A. Aziz, K. L. Narasimhan, N. Periasamy, P. S. Meenakshi, and S. Wategaonkar, "On the assignment of the absorption bands in the optical spectrum of Alq3," Synthetic Met. **126**, 199 – 205 (2002).
23. G. McAdam, P. J. Newman, I. McKenzie, C. Davis, and B. R. W. Hinton, "Fiber optic sensors for detection of corrosion within aircraft," Struct. Health Monit. **4**, 47 – 56 (2005).
24. J. Ščančar and R. Milačič, "Aluminium speciation in environmental samples: a review," Anal. Bioanal. Chem. **386**, 999 – 1012 (2006).
25. R. Kostecki, H. Ebendorff-Heidepriem, S. C. Warren-Smith, and T. M. Monro, "Predicting the drawing conditions for microstructured optical fiber fabrication," Opt. Mater. Express **4**, 29 – 40 (2014).
26. H. Ebendorff-Heidepriem, S. C. Warren-Smith, and T. M. Monro, "Suspended nanowires: fabrication, design and characterization of fibers with nanoscale cores," Opt. Express **17**, 2646 – 2657 (2009).
27. G. Brambilla, F. Xu, and X. Feng, "Fabrication of optical fibre nanowires and their optical and mechanical characterisation," Electron. Lett. **42**, 517 – 519 (2006).
28. G. Zhai and L. Tong, "Roughness-induced radiation losses in optical micro or nanofibers," Opt. Express **15**, 13805 – 13816 (2007).
29. M. Fujiwara, K. Toubaru, and S. Takeuchi, "Optical transmittance degradation in tapered fibers," Opt. Express **19**, 8596 – 8601 (2011).
30. S. C. Warren-Smith, E. Sinchenko, P. R. Stoddart, and T. M. Monro, "Distributed fluorescence sensing using exposed core microstructured optical fiber," IEEE Photon. Technol. Lett. **22**, 1385 – 1387 (2010).
31. G. S. He, H. Qin, and Q. Zheng, "Rayleigh, Mie, and Tyndall scatterings of polystyrene microspheres in water: Wavelength, size, and angle dependences," J. Appl. Phys. **105**, 023110 (2009).
32. P. J. Roberts, F. Couny, H. Sabert, B. J. Mangan, D. P. Williams, L. Farr, M. W. Mason, A. Tomlinson, T. A. Birks, J. C. Knight, and P. S. Russell, "Ultimate low loss of hollow-core photonic crystal fibres," Opt. Express **13**, 236 – 244 (2005).
33. K. Tajima, J. Zhou, K. Nakajima, and K. Sato, "Ultralow loss and long length photonic crystal fiber," J. Lightwave Technol. **22**, 7 – 10 (2004).
34. T. Kaino, M. Fujiki, S. Oikawa, and S. Nara, "Low-loss plastic optical fibers," Appl. Opt. **20**, 2886 – 2888 (1981).
35. T. Seydel, A. Madsen, M. Tolan, G. Grübel, and W. Press, "Capillary waves in slow motion," Phys. Rev. B **63**, 073409 (2001).
36. J. Jäckle and K. Kawasaki, "Intrinsic roughness of glass surfaces," J. Phys. - Condens. Mat. **7**, 4351 – 4358 (1995).
37. S. C. Xue, M. C. J. Large, G. W. Barton, R. I. Tanner, L. Poladian, and R. Lwin, "Role of material properties and drawing conditions in the fabrication of microstructured optical fibers," J. Lightwave Technol. **24**, 853 – 860 (2006).
38. J. Liu, H. Li, and J.-M. Lin, "Measurements of surface tension of organic solvents using a simple microfabricated chip," Anal. Chem. **79**, 371 – 377 (2007).
39. K. Boyd, H. Ebendorff-Heidepriem, T. M. Monro, and J. Munch, "Surface tension and viscosity measurement of optical glasses using a scanning CO_2 laser," Opt. Mater. Express **2**, 1101 – 1110 (2012).

1. Introduction

Exposed-core microstructured optical fibers (MOFs) made from silica open up new opportunities for creating sensors capable of withstanding long term use in harsh environments and for providing real time analysis anywhere along the fiber length [1]. The portion of guided light extending from the glass core, often described as 'evanescent field', is affected by the refractive index and absorption characteristics of the medium surrounding it [2,3]. This light-matter overlap provides opportunities for exploiting the interaction of light with gases and liquids, where absorption and/or fluorescence can be used to determine the composition and concentration of the analyte [4,5].

Although sensor molecules provide a method for fluorescence based analyte detection [6], existing staining and/or specimen sampling based methodology is not well suited for real-time, in situ, and/or remote sensing applications. For such applications it is necessary to immobilize sensor molecules on the glass surface of the MOF exposed core, which can then be used directly within the medium as a sensor without requiring prior pre-mixing of analyte with sensor molecules. Functionalization methods traditionally used include silanes [7,8] or polyelectrolytes [9,10], which provide a functional group on the surface to which the sensor molecules can be covalently attached. These processes require several steps that typically take many hours to perform, due to the incubation times needed to achieve consistent maximized binding efficiency [8,10]. Some important factors to consider when choosing a functionalization method are the conditions in which the sensor is to be used (for example polyelectrolytes have been found to wash off in acidic conditions [11]), and any additional optical losses that might occur as a result. Also, achieving uniform covalent binding of the sensor molecules along the constrained surface of MOFs in a consistent manner is challenging using silanes or polyelectrolytes [5,8], since results are highly dependent on experimental conditions (temperature, concentration, solvents, hydration and reaction time) as well as pre- and post-treatment processes [5,10–12]. These factors can diminish sensor performance, reducing the achievable light-matter interactions, which in turn decreases sensitivity.

Both polymer and silica have properties that make them attractive for optical fiber sensing applications [13,14]. Poly(methyl methacrylate) (PMMA) polymer optical fibers (POFs) have high elastic strain limits, high fracture toughness, and high flexibility in bending, however high attenuation properties and difficulties with splicing, cleaving and coupling makes small core size POF sensors challenging [14–17]. On the other hand, silica is known to be reliable under a range of processing and use environments, with relatively better mechanical and thermal stability [13]. Highly homogeneous, high purity bulk material is commercially available, which has led to the development of low loss silica telecom fibers [18]. Silica has a relatively low refractive index, which can improve the sensitivity of evanescent field sensors, since reducing the index contrast (Δn) at the core-cladding boundary increases the power fraction to the analyte or functionalized surface [19]. Also, silica exposed-core MOF fibers can be spliced to single mode fiber for improved handling and integration with commercial interrogation units [20].

In this paper we demonstrate a one step functionalization process for optical fiber sensing applications, by applying thin film ($\sim$50 nm) PMMA doped with sensor molecules to a silica exposed-core MOF. This integrates the polymer, silica and sensor molecule elements to create a distributed sensor capable of detecting an analyte of interest anywhere along the fiber's length, while removing the need for surface attachment of functional groups. We show that the thin film coating also serves a protective function, which has the potential to solve some of the practical issues involved in functionalizing exposed-core MOFs where sensitivity to the chosen analyte as well as environmental protection is required. We also characterize the attenuation properties of the thin film functionalized fiber, and analyze the overall loss of the polymer layer. By normalizing the fiber loss before and after adding the polymer layer to the field distribution, we are

able to determine the source of added attenuation to be primarily due to surface roughness.

2. One step functionalization process

The method used to coat silica exposed-core MOFs with PMMA is an extension of the method used for micron scale polymer coating in glass capillaries [21]. A clear cast acrylic rod (PMMA) with a density of 1.18 g/cm^3, also known as a 'plexiglass rod' (Professional Plastics Pte. Ltd. [Singapore]), was dissolved in dichloromethane (DCM) at a concentration of 12.3 g/L. 8-hydroxyquinoline (8-HQ), which is known to complex with aluminum ions (Al cations) and then fluoresce strongly with UV excitation [22], was dissolved in DCM and added to the dissolved PMMA solution making a concentration of $30_{(8\text{-HQ})} : 100_{(\text{PMMA})}$ by weight. The detection of Al cations is of particular interest as it provides a marker of aluminum corrosion [23] and is also an environmental hazard [24]. One end of the fabricated [25] silica exposed-core MOF (Fig. 1(a)), with an effective core diameter of 7.5 μm (defined as the diameter of a circle whose area is equal to a triangle that fits wholly within the core area [26]), was fed through a silicon septa fitted to the bottom of an open-end vial. This setup, shown by the schematic in Fig. 1(b), was then used to coat the outside of the MOF including the exposed core region. The PMMA+8-HQ DCM solution was placed into the vial (∼5 mm depth), and the fiber was pulled through the solution and silicon septa by hand (at ∼8 m/min) to leave behind a ∼50 nm coating of the doped PMMA on the core surface (Fig. 1(c)). Uniformity of the polymer layer is critically important for optical performance of the device. Measured results from scanning electron microscope (SEM) images of six samples, from the center and 10 cm in from the ends of two individually coated 1 m lengths of fiber, showed the coating thickness on the outside edge of the exposed-core to be in the range 43–46 nm with measurement uncertainty of ±9 nm. The coating procedure was performed in a laboratory chemical fume hood at room temperature (∼21°C), without additional curing.

3. Characterization of thin film polymer layer

3.1. Sensing measurements

To test the ability of the coated fiber to detect Al cations, an 18 mW laser excitation light source with a wavelength of 375 nm was coupled into the core of an 80 cm long PMMA+8-HQ functionalized fiber using an aspheric lens (f=2.75 mm, NA=0.55) via a dichroic mirror. The back

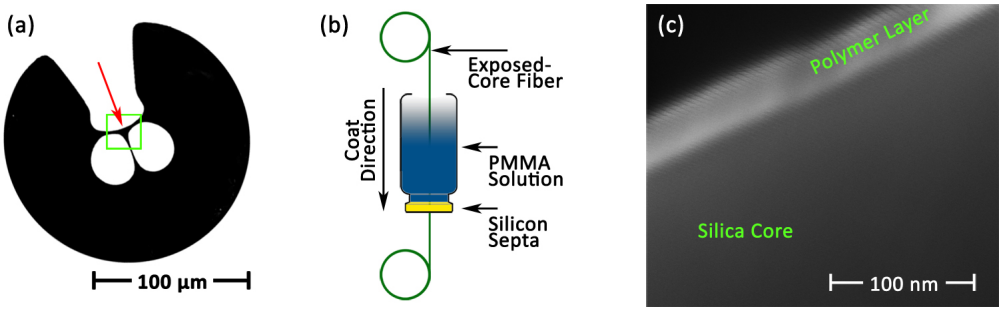

Fig. 1. (a) Contrast enhanced SEM image of (silica material shown in black) exposed-core MOF cross section, having an effective core diameter of 7.5 μm (core location shown by green box). (b) A schematic of the thin-film polymer coating method used to coat the outside of the MOF including the exposed core region. (c) Close-up SEM of the outside edge of the exposed core (red arrow in Fig. 1(a)) with 50 nm polymer coating (light grey).

reflected light collected from the coated fiber core was imaged using the same lens, passed through the dichroic mirror, 425 nm long pass filter and $\times 4$ objective, and characterized using a Horiba iHR550 Imaging Spectrometer with Synapse CCD Detector. The exposed-core region of the coupled fiber was then exposed to Al cations by immersing the outside of a 23 cm long central section of the fiber in a saturated solution of potassium aluminum sulfate (potassium alum, $KAl(SO_4)_2 \cdot 12H_2O$), and the back reflected spectra were measured immediately after immersion and again after 1 hour of immersion. The setup is shown by the schematic in Fig. 2(a). The measured result before immersion subtracted from the after immersion results is presented in Fig. 2(b), which shows the fluorescence peak of 8-HQ complexed with Al cations [22] increasing over time. This result demonstrates the ability of a thin polymer film functionalized fiber to detect Al cations, with the potential for corrosion detection, and confirms sufficient mobility of the 8-HQ within the polymer matrix to allow complexation with the Al cations.

3.2. Air exposure induced deterioration

The impact of deterioration on the transmission properties of the functionalized fiber, resulting from exposing the functionalized fiber to air, was measured using the same procedure detailed in [1] which is briefly outlined here. A 4 m long PMMA+8-HQ functionalized fiber was coupled to a 100 W halogen broadband source with an approximately Gaussian-distributed intensity profile and peak power at 800 nm. At the other end, the light from the core was imaged onto the detector of an Ando AQ6315E Optical Spectrum Analyzer (OSA) and the transmitted power spectrum, in dBm, was recorded from 350–1750 nm every two minutes. This procedure was performed in a laboratory at room temperature ($\sim$21°C), with the fiber in air, where the setup was left long enough ($\sim$6 hours) so that the measured power stabilized to within $\pm$0.05 dBm, then used to take time based measures of the power for 180 hours. Any changes over time (t)

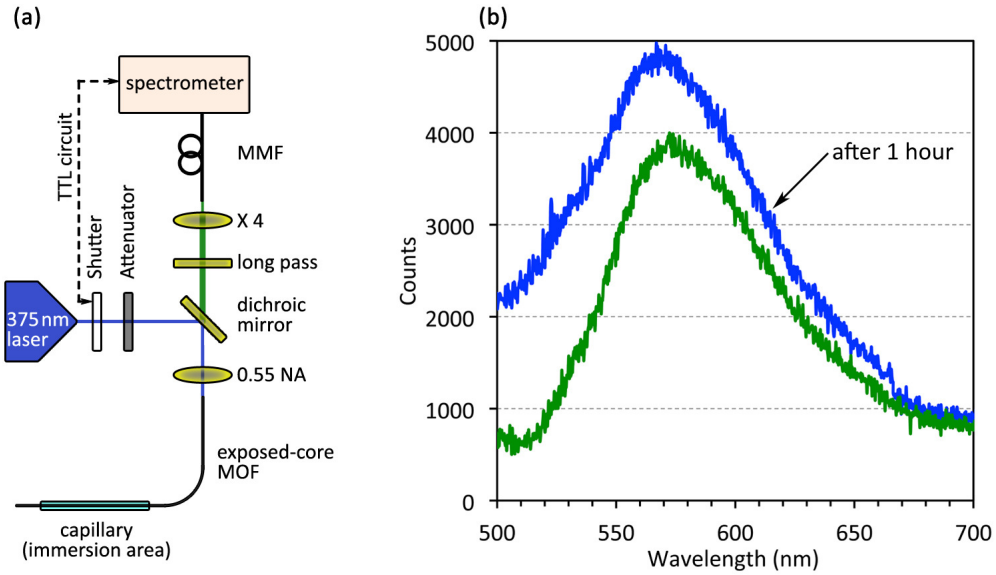

Fig. 2. (a) Setup used to test the ability of the coated fiber to detect Al cations (MMF is multimode fiber). (b) Back reflected spectra of the functionalized fiber directly after immersion in Al cations solution (green – ●) and after 1 hour of immersion in solution (blue – ●).

in the transmission characteristics were then fitted to the equation,

$$P(\lambda,t) = P(\lambda,0)10^{-\xi tz/10} \tag{1}$$

where ξ is the loss in dB $m^{-1}day^{-1}$ and z is the fiber length in meters. For comparison the result in [1] for an uncoated exposed-core MOF, with 10 μm core diameter, is shown by the red line in Fig. 3. The result of $\xi(\lambda)$ (Eq. (1)) for the thin-film functionalized fiber, shown by the blue line in Fig. 3, shows a significant improvement compared to the uncoated fiber.

This deterioration in the transmission properties is expected to come from changes in the mechanical and/or compositional characteristics at the core surface, causing light scattering effects [27–29]. When the core diameter is reduced these light scattering effects are expected to increase, as a greater portion of guided light travels outside the core. However, this result shows less deterioration in transmission properties even though the core diameter of this functionalized fiber is smaller (7.5 μm) compared to the uncoated exposed-core MOF from [1] (10 μm). This shows that the thin film coating is providing a protective function for the core surface. For example, at $\lambda = 532$ nm the air induced deterioration in the transmission properties of the thin-film functionalized fiber (3×10^{-3} dB $m^{-1}day^{-1}$) is an order of magnitude better than for the previously reported uncoated result [1]. This is significant for optical fiber sensors requiring long term and/or harsh environmental applications while providing long length light interaction with the analyte of interest.

3.3. Functionalized fiber loss

To determine the impact of polymer coating on propagation loss, cutback fiber loss measurements were performed using a 100 W halogen broadband source with an approximately Gaussian-distributed intensity profile and peak power at 800 nm. The before and after polymer coating loss measurements are shown by the blue and red lines in Fig. 4 respectively, and

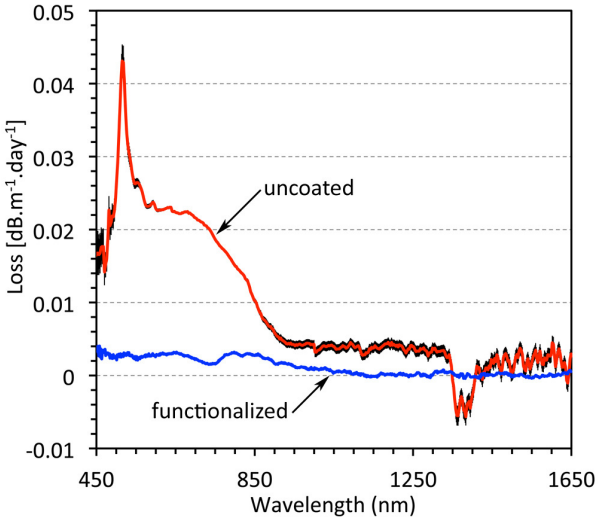

Fig. 3. Deterioration in the transmission properties of the air exposed uncoated (red – ●, from [1] with 10 μm core diameter) and thin-film polymer functionalized (blue – ●) silica exposed-core MOF. The 95% confidence interval is shown in black. For the thin-film polymer functionalized fiber result, the confidence interval is approximately the same as the line thickness.

summarized in Table 1 for 532 nm, 1064 nm, and 1550 nm wavelengths. These results show an increase of ∼10–20 times after applying the polymer layer. The difference between these coated and uncoated fiber loss measurements ($\alpha_{\text{after}} - \alpha_{\text{before}}$) is shown by the green line in Fig. 4.

Understanding the reasons the polymer layer adds to the overall loss, and finding ways to reduce these losses, can significantly improve the distributed sensor practical range [30]. The loss of a fiber is given by,

$$\alpha_{\text{fiber}}(\lambda) = \left(\frac{\varepsilon_0}{\mu_0}\right)^{\frac{1}{2}} \frac{\int_\infty n^{\text{r}} \alpha |\mathbf{E}|^2 \, \mathrm{d}A}{\int_\infty \mathbf{E} \times \mathbf{H}^* \cdot \hat{\mathbf{z}} \, \mathrm{d}A} \tag{2}$$

where $n^{\text{r}}(x,y)$ and $\alpha(x,y)$ are the refractive index and material loss distribution, $\mathbf{E}(x,y)$ and $\mathbf{H}(x,y)$ are the electric and magnetic field distributions, and $\mathbf{z}$ is along the optical axis of the fiber. This guided mode loss includes all loss mechanisms, such as absorption and scattering. The change in loss of the guided mode due to the addition of the polymer layer can be written

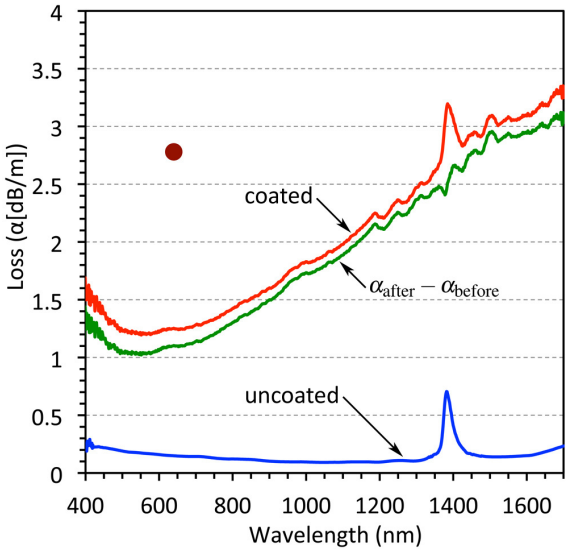

Fig. 4. Broadband cutback loss measurements of silica exposed-core MOF, before (blue – ●) and after polymer (PMMA+8HQ) coating (red – ●). The difference between the coated and uncoated fiber loss $\alpha_{\text{after}} - \alpha_{\text{before}}$ is shown in green (– ●). Cutback loss measurement at $\lambda = 640$ nm for un-doped PMMA coated exposed-core MOF (dark-red dot ●).

Table 1. Loss measurements for silica exposed-core MOF (Fig. 1(a))

Wavelength (nm)	Uncoated (dB/m)	Coated (dB/m)
532	0.178	1.04
1064	0.092	1.82
1550	0.141	2.94

as,

$$\alpha_{\text{after}} - \alpha_{\text{before}} = \left(\frac{\varepsilon_0}{\mu_0}\right)^{\frac{1}{2}} \frac{\int_{\text{layer}} n^{\text{r}} \alpha |\mathbf{E}|^2 \, \mathrm{d}A}{\int_{\infty} \mathbf{E} \times \mathbf{H}^* \cdot \hat{\mathbf{z}} \, \mathrm{d}A} \tag{3}$$

where we have assumed the mode distribution has not changed due to addition of the layer, since it is very thin (~ 50 nm). In Eq. (3), $\alpha(x,y)$ includes loss of polymer material, α_{m}, and any loss due to scattering or inhomogeneity added during fabrication, α_{f}, hence $\alpha(x,y) = \alpha_{\text{m}} + \alpha_{\text{f}}(x,y)$. As a result, Eq. (3) can be rewritten as,

$$\alpha_{\text{after}} - \alpha_{\text{before}} = \left(\frac{\varepsilon_0}{\mu_0}\right)^{\frac{1}{2}} \left(\frac{n_{\text{m}}^{\text{r}} \, \alpha_{\text{m}} \int_{\text{layer}} |\mathbf{E}|^2 \, \mathrm{d}A}{\int_{\infty} \mathbf{E} \times \mathbf{H}^* \cdot \hat{\mathbf{z}} \, \mathrm{d}A} + \frac{\int_{\text{layer}} n^{\text{r}}(x,y) \alpha_{\text{f}}(x,y) |\mathbf{E}|^2 \, \mathrm{d}A}{\int_{\infty} \mathbf{E} \times \mathbf{H}^* \cdot \hat{\mathbf{z}} \, \mathrm{d}A} \right) \tag{4}$$

or alternatively,

$$\begin{aligned} &\left(\frac{\mu_0}{\varepsilon_0}\right)^{\frac{1}{2}} \frac{(\alpha_{\text{after}} - \alpha_{\text{before}}) \int_{\infty} \mathbf{E} \times \mathbf{H}^* \cdot \hat{\mathbf{z}} \, \mathrm{d}A}{n_{\text{m}}^{\text{r}} \int_{\text{layer}} |\mathbf{E}|^2 \, \mathrm{d}A} \\ &= \alpha_{\text{m}} + \frac{\int_{\text{layer}} n^{\text{r}}(x,y) \alpha_{\text{f}}(x,y) |\mathbf{E}|^2 \, \mathrm{d}A}{n_{\text{m}}^{\text{r}} \int_{\text{layer}} |\mathbf{E}|^2 \, \mathrm{d}A} \\ &= \alpha' \end{aligned} \tag{5}$$

where α' is the overall layer loss. Equation (5) can be used to determine the loss induced from applying the polymer layer, as a function of the guided mode field distribution fraction, by measuring $\alpha_{\text{after}} - \alpha_{\text{before}}$ and calculating electric and magnetic fields of the fiber propagation mode. To calculate the electric and magnetic fields, numerical simulation was performed on the fiber core profile taken from an SEM image, with a 50 nm polymer layer added to the

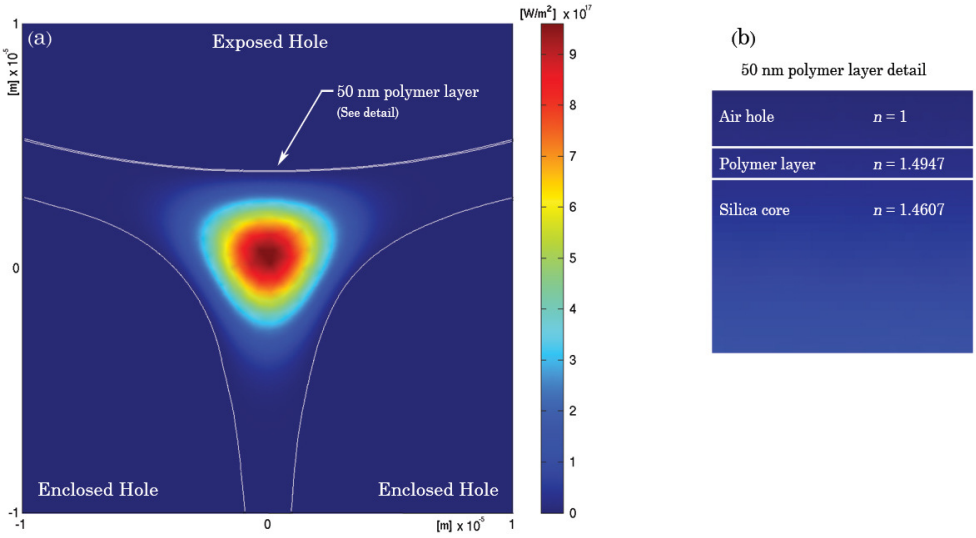

Fig. 5. (a) Numerical simulation result for the z-component power flow ($\mathbf{S}_z$) distribution at $\lambda = 532$ nm of the fundamental mode using full vector FEM. The fiber core profile (shown by white outline) taken from SEM image. (b) Detail of the of the refractive index profile used for the simulation.

exposed hole side of the core, using full vector finite element method (FEM) in the commercial package COMSOL 3.4. For example, Fig. 5(a) shows the FEM result for the z-component power flow ($\mathbf{S}_z = \mathbf{E}\times\mathbf{H}^*\cdot\hat{\mathbf{z}}$) distribution at $\lambda = 532$ nm of the fundamental mode, with refractive indices of the air holes, silica core, and polymer layer being $n_{\text{holes}} = 1$, $n_{\text{silica}} = 1.4607$, and $n_{\text{layer}} = 1.4947$ respectively (Fig. 5(b)). The cutback measurements (see Fig. 4) were used together with the fundamental mode FEM calculations with silica and PMMA material wavelength dependent refractive indices (n_{m}^{r}) to determine α' for 405 nm, 532 nm, 640 nm, 790 nm, 980 nm, 1064 nm, and 1550 nm wavelengths. The green dots in Fig. 6 plot the results for these seven wavelengths which show a trend of reducing attenuation with increased wavelength. To investigate this λ dependence, α' was fitted to the function,

$$\alpha' = \sum_{i=0}^{4} \frac{a_i}{\lambda^i} \tag{6}$$

which revealed the experimental values of α' could be fitted with either of the following two functions,

$$\alpha'_1 = \left(\frac{2049.04}{\lambda} + \frac{413.27}{\lambda^4} + 6988.35\right) \qquad \left[R^2 = 0.997\right] \tag{7}$$

$$\text{and} \qquad \alpha'_2 = \left(\frac{1272.97}{\lambda^3} + 8001.75\right) \qquad \left[R^2 = 0.994\right] \tag{8}$$

with λ in μm, and α' in dB/m units, shown by the red and blue lines respectively in Fig. 6. The fit of these functions could not be improved by allowing $a_2 \neq 0$.

Equation (7) shows wavelength dependencies of the form known to originate from intrinsic material light scattering. In general terms, material density changes cause intrinsic light scattering which is termed as Tyndall, Mie, and Rayleigh scattering originating from constituents

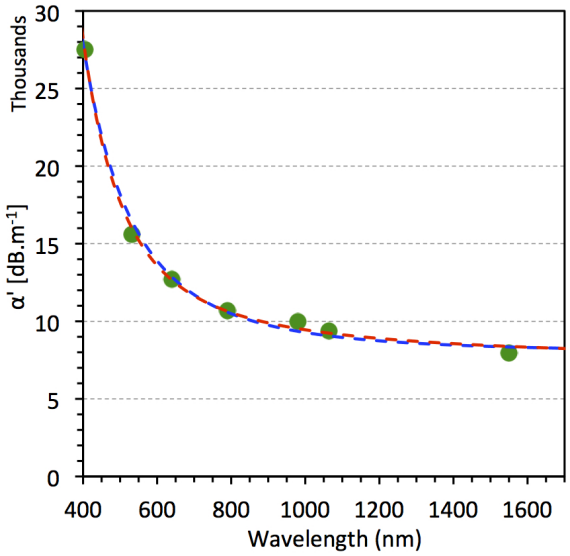

Fig. 6. (green ●) Plot of loss induced from applying the polymer layer, α' in Eq. (5), using cutback measurements ($\alpha_{\text{after}} - \alpha_{\text{before}}$, Fig. 4) for 405 nm, 532 nm, 640 nm, 790 nm, 980 nm, 1064 nm, and 1550 nm wavelengths. Plot of fitted λ dependent functions Eq. (7) (red - - ■) and Eq. (8) (blue - - ■).

of sizes $r > 40\lambda$, $\lambda/20 < r < 40\lambda$, and $r < \lambda/20$ respectively [31]. On the other hand, Eq. (8) has λ^{-3} dependence which is described by Roberts *et al.* [32] as applying to surface roughness at all length scales. For suspended and free-standing nanowires, increased field strength at the surface leading to larger roughness scattering type loss [28, 33] has also been shown to have core size dependence of $\alpha \propto d^{-3}$ [26].

The fact that both functions α_1' and α_2' fit the experimental data indicates that any function α' given by $\alpha' = \rho\alpha_1' + (1-\rho)\alpha_2'$ where $\rho \in [0,1]$ fits the data as well. In order to determine ρ, we compare the coefficient of Rayleigh scattering that has been measured for bulk PMMA [34] with the coefficient of λ^{-4} in Eq. (7), which appears to be 5×10^6 times bigger than actual value as reported in [34]. To investigate the possibility that the added 8-HQ is contributing to additional Rayleigh scattering, another length of the exposed-core MOF was coated with a thin film ($\sim$ 50 nm) of un-doped PMMA using the same method as described above. The loss of this PMMA coated exposed-core MOF was measured at $\lambda = 640$ nm using the cutback method, which was found to be 2.78 dB/m compared to 1.25 dB/m measured for the PMMA+8-HQ, shown by the dark-red dot and red line in Fig. 4 respectively. This reveals that 8-HQ is not the cause of the additional loss from the thin film layer, instead helping to reduce the overall attenuation. Also, the λ^{-1} Mie type scattering in Eq. (7) cannot be due to intrinsic properties of the thin film, since this would suggest constituents with sizes orders of magnitude larger then the layer thickness. This implies that $\rho \approx 0$, since Eq. (7) cannot be describing intrinsic material properties of the thin film layer as being the predominant cause for the additional loss, and so does not contribute to the loss function α' in terms of intrinsic material light scattering.

To investigate surface roughness scattering type loss described by Eq. (8), a ContourGT-K1 coherence scanning interferometer was used to measure the roughness of the exposed-core MOF core surface before and after polymer coating. Before coating the roughness along a 20 μm length of the core was found to be $S_z = 0.394$ nm, whereas after coating $S_z = 0.873$ nm. The additional measured roughness at the core surface, together with Eq. (8) having an $\alpha \propto \lambda^{-3}$ dependence [32], indicates that the source of the added attenuation from the polymer layer is primarily due to surface roughness. Such roughness has been shown to arise from excited surface capillary waves (SCWs) [32], where small ripples on the surface are frozen in at the time of fiber fabrication. The amplitude of SCWs is dictated by equilibrium thermodynamics with surface tension (γ) providing a restoring force. During material phase transition these SCWs freeze [35], leaving a surface roughness proportional to inverse surface tension ($S_z \propto \gamma^{-1}$) [32,36]. Both the PMMA ($\gamma = 0.032$ Nm^{-1} [37]) and DCM ($\gamma = 0.026$ Nm^{-1} [38]) used for the thin film coating have surface tensions an order of magnitude lower than for the silica ($\gamma = 0.31$ Nm^{-1} [39]) used to fabricate the exposed-core MOF. This relatively low surface tension for the polymer coating gives rise to higher amplitude SCWs, leading to additional surface roughness and therefore additional loss. Hence, improvements may be possible by finding ways to increase the surface tension of polymer mixtures used for the thin film coating.

4. Conclusion

By applying a thin polymer film ($\sim$50 nm) doped with sensor molecules to a silica exposed-core MOF, a one step functionalizing process for optical fiber sensing applications has been demonstrated, which eliminates the need for functional groups on the core surface for sensor molecule attachment and offers the prospect of being applied during the fiber drawing process. This method integrates the polymer, silica, and sensor molecule properties to create a distributed sensor capable of detecting an analyte of interest anywhere along the fiber length. The technique was successfully applied to the detection of Al cations in solution by doping the PMMA film with 8-HQ sensing molecules showing sufficient mobility in the PMMA matrix to allow interaction of the sensing molecules with the analyte of interest. This sensing reaction has

the potential to be applied to corrosion and environmental hazard detection where the benefits of a distributed sensor are significant.

The air induced deterioration in transmission properties of the coated exposed-core MOF was shown to be an order of magnitude reduced compared to the previously reported un-coated result. The protective function of this coating is a practical improvement for any use of these fibers, particularly for photonic applications were environmental protection is needed while maintaining access to the guided light. This improvement is attributed to the polymer matrix, however further work is needed to understand if the sensor molecules influence the protective function.

Cutback loss measurements showed an increase in the attenuation of $\sim$10–20 times after applying the polymer layer. Analyzing the overall loss of the polymer layer, by calculating the field distribution normalized attenuation of the layer, we were able to determine that the source of the added attenuation from the polymer layer is primarily due to surface roughness. Such roughness arises from excited SCWs, which become frozen in during material phase transition. Further work is needed to find ways of improving the functionalized surface, compare other surface coating methods, and exploit the method for more complex sensing molecules and applications.

Acknowledgments

The authors acknowledge Peter Henry and Stephen Warren-Smith for their contribution to the silica fiber drawing, Kristopher Rowland and Sabrina Heng for helpful discussions, and Adelaide Microscopy for micrograph support. This work was performed in part at the OptoFab node of the Australian National Fabrication Facility, which provides nano and microfabrication facilities for Australia's researchers, utilizing Commonwealth and SA State Government funding. Tanya Monro acknowledges the support of an ARC Laureate Fellowship.